Tricyclic Farnesyl Protein Transferase Inhibitors: Crystallographic and Calorimetric Studies of Structure−Activity Relationships†

Corey L. Strickland, Patricia C. Weber,* William T. Windsor, Zhen Wu, Hung V. Le, Margaret M. Albanese, Carmen S. Alvarez, David Cesarz, Joycelyn del Rosario, Jeffrey Deskus, Alan K. Mallams, F. George Njoroge, John J. Piwinski, Stacy Remiszewski, Randall R. Rossman, Arthur G. Taveras, Bancha Vibulbhan, Ronald J. Doll, Viyyoor M. Girijavallabhan, and Ashit K. Ganguly

Departments of Structural Chemistry and Chemical Research, Schering-Plough Research Institute, Kenilworth, New Jersey 07033

Received January 21, 1999

Crystallographic and thermodynamic studies of farnesyl protein transferase (FPT) complexed with novel tricyclic inhibitors provide insights into the observed SAR for this unique class of nonpeptidic FPT inhibitors. The crystallographic structures reveal a binding pattern conserved across the mono-, di-, and trihalogen series. In the complexes, the tricycle spans the FPT active site cavity and interacts with both protein atoms and the isoprenoid portion of bound farnesyl diphosphate. An amide carbonyl, common to the tricyclic compounds described here, participates in a water-mediated hydrogen bond to the protein backbone. Ten high-resolution crystal structures of inhibitors complexed with FPT are reported. Included are crystallographic data for FPT complexed with SCH 66336, a compound currently undergoing clinical trials as an anticancer agent (SCH 66336, 4-[2-[4-(3,10-dibromo-8-chloro-6,11-dihydro-5*H*-benzo[5,6]-cyclohepta[1,2-*b*]pyridin-11-yl)-1-piperidinyl]-2-oxoethyl]-1-piperidinecarboxamide). Thermodynamic binding parameters show favorable enthalpies of complex formation and small net entropic contributions as observed for 4-[2-[4-(3,10-dibromo-8-chloro-6,11-dihydro-11*H*-benzo-[5,6]cyclohepta[1,2-*b*]pyridin-11-ylidene)-1-piperidinyl]-2-oxoethyl]pyridine *N*-oxide where $\Delta H°_{bind} = -12.5$ kcal/mol and $T\Delta S°_{bind} = -1.5$ kcal/mol.

Introduction

The use of mechanism-based inhibitors is a relatively new therapeutic approach for the treatment of cancer. The rationale for this approach arises from discoveries in the molecular processes by which cells regulate growth. For example, nearly one-third of all forms of cancer result from the unregulated activity of ras proteins.[1] Detailed studies of the ras protein demonstrated that specific C-terminal posttranslational modifications were required for its ability to transform cells.[2] In the early 1990s, farnesyl protein transferase (FPT), one of several essential ras-modifying enzymes, was discovered.[3] FPT catalyzes attachment of the 15-carbon isoprenoid from farnesyl diphosphate (FPP) to the cysteine side chain of a conserved CaaX sequence located at the carboxy terminus of ras.[4,5] Further characterization of the enzyme suggested that specific inhibition of FPT may prove an effective anticancer strategy.[6,7] This possibility has prompted extensive research aimed at discovery of potent FPT inhibitors.

Novel, nonpeptidic FPT inhibitors discovered at Schering-Plough are characterized by a tricycle core composed of two six-membered aromatic rings fused to a central seven-membered ring.[8−14] Structural features for classes of inhibitors discussed here are shown in Figure 1. SCH 44342 (**1**) is a representative example and constituted an early lead in the FPT inhibitor program ($IC_{50} = 250$ nM[14]). Elaboration to optimize affinity and selectivity resulted in molecules with FPT inhibition constants in the low-nanomolar range and >10 000-fold selectivity over the structurally related geranylgeranyl protein transferase.[8] The tricyclic FPT inhibitor, SCH 66336, 4-[2-[4-(3,10-dibromo-8-chloro-6,11-dihydro-5*H*-benzo-[5,6]cyclohepta[1,2-*b*]pyridin-11-yl)-1-piperidinyl]-2-oxoethyl]-1-piperidinecarboxamide (**2**), is undergoing clinical trials as an anticancer agent[8,15] and represents one of the first members of this class of noncytotoxic anticancer agents to enter clinical trials.

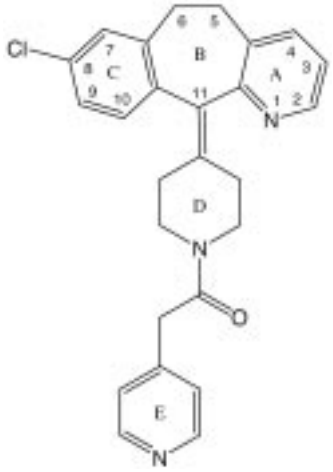

Figure 1. Chemical structure of tricyclic FPT inhibitors. Rings are labeled for clarity.

* Corresponding author: Patricia C. Weber, Schering-Plough Research Institute, 2015 Galloping Hill Rd, K-15-3-3855, Kenilworth, NJ 07033-0539. Tel: (908) 740-3426. Fax: (908) 740-7305. E-mail: patricia.weber@spcorp.com.

† Abbreviations: farnesyl protein transferase (FPT), farnesyl diphosphate (FPP), concentration of inhibitor to cause 50% inhibition (IC_{50}), structure−activity relationship (SAR), isothermal titration calorimetry (ITC), α-hydroxyfarnesylphosphonic acid (αHFP).

10.1021/jm990030g CCC: $18.00
Published on Web 06/02/1999

FPT is an obligatory dimer composed of α- and β-subunits. The crystal structure of unliganded FPT[16] showed that the α-subunit is composed of seven pairs of antiparallel α-helices packed adjacent to each other to form a crescent shape. The six pairs of helices in the β-subunit are arranged as a double-walled barrel. The active site cavity is situated near the center of the molecule and lined with residues of both subunits. The catalytic zinc is liganded by three side chains arising from the β-subunit. The fourth ligation site is occupied by a water molecule.

The FPT active site cavity, which binds FPP and the carboxy terminal residues of the ras protein, is much larger than a single tricycle inhibitor. The large size of the cavity confounded attempts to define the bound conformation of the inhibitor by molecular modeling alone. Crystallographic studies were initially undertaken to determine in detail the intermolecular interactions between FPT and inhibitors. Subsequent structural studies revealed conserved interactions and were used to formulate a structural basis for understanding the relationship between small molecule structure and in vitro activity for compounds synthesized in the FPT inhibitor program.

Analysis of the tricycle inhibitor SAR patterns showed several consistent features. For example, selective addition of halogens at the 3 and 10 positions of the tricycle moiety (rings A and C, Figure 1) increased inhibitor affinity. Typically, 2.5−10-fold increases were observed following incorporation of a second halogen at the 3 position,[9,13] and additional 25−40-fold increases were found when the third halogen was added to the phenyl ring (ring C) in either the 7 or 10 position.[8] Second, inclusion of hydrogen-bonding capabilities such as an amide carbonyl between rings D and E and a pyridinyl nitrogen in the tricycle improved inhibitor potency.[10] Third, relatively large structural variations in ring E substituents were tolerated, although 4-substituted pyridines and piperidines gave the highest potencies.[9,13]

Despite several consistent trends, other features of the SAR were unclear. In particular, the preferred chirality at C-11 differed among the series. The C-11 *S* conformation exhibited 4-fold greater potency in the 8-chloro series (**3** and **4**, Table 1). Within the 3-Br, 8-Cl series (**5** and **6**), compounds having either the *R* or *S* configuration at C-11 were equipotent (Table 1). However in the trihalogen series (**2** and **8**−**10**), there is a 100-fold difference in potency between inhibitors having the *R* and *S* configurations at C-11. From the chemical structure of the inhibitor alone, it was also not immediately apparent why in the mono-, di-, and trihalogen series compounds having a double bond between rings B and D (**1**, **7**, and **8**) were as potent as compounds with a stereochemical center at C-11 (Table 1). Structural studies were undertaken to clarify these intriguing features of the SAR.

The thermodynamic parameters of binding were determined to understand the enthalpy and entropy compensations involved in transfer of the compounds from solution to the FPT active site. Such experimental information has been previously shown to effectively complement structure-based inhibitor design.[17−22] In this system, where the inhibitors have few rotatable bonds, knowledge of the overall entropy of binding provides an indication of the extent to which the solution and bound conformations are similar. In addition, the entropy of binding assists evaluation of the importance of solvent displacement in inhibitor elaboration.

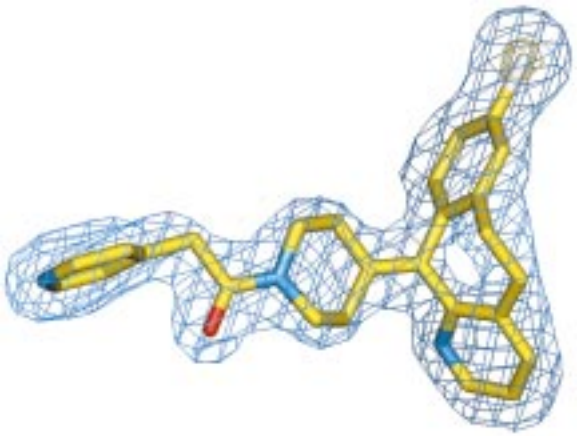

Figure 2. Omit electron density[35] for SCH 44342. Blue and yellow lines show 1.9σ and 10.0σ electron density values, respectively. Electron densities of this clarity were routinely observed for the FPT:FPP:inhibitor complexes.

Results

Visualization of Tricyclic Inhibitors. Electron density maps clearly show the bound conformation and location of **1** in the FPT active site cavity (Figure 2). The presence of a higher molecular weight halogen atom in the molecule assists in unambiguous definition of inhibitor binding mode and refinement of atomic positions. In the initial 2.1 Å $(F_o - F_c)\alpha_{calc}$ electron density map, the position of the 8-chlorine was indicated by an 11σ peak, and the C-5 and C-6 positions within the seven-membered B ring were clearly defined. The electron density accounts for all atoms of SCH 44342. In the refined structure, the inhibitor is well-ordered with an average *B*-factor of 22 Å^2 (Table 1).

Inhibitor Binding Site and Overall Conformation. The inhibitor SCH 44342 binds in the center of the FPT active site cavity (Figure 3). The tricycle portion (rings A, B, and C) is situated deep in the cavity, while ring E is closest to the molecular surface. The piperidine and pyridinyl rings (rings D and E) extend from the tricycle. As a result, the bound conformation of SCH 44342 resembles the two-dimensional representation in Figure 1 except that, in three dimensions, the tricycle moiety is at nearly right angles to the remainder of the inhibitor.

Interactions of Inhibitor with FPT. The crystallographic studies revealed extensive interactions between **1** and FPT. The pyridinyl ring of the tricycle (ring A, Figure 1) binds in a pocket lined with several aromatic side chains (Figure 4). The ring forms two edge-to-face interactions with FPT, acting as a donor ring with Trp102β and as the acceptor ring for Trp106β. The pyridinyl nitrogen makes a 2.9 Å hydrogen bond to a water molecule, which is in turn hydrogen-bonded to the Ser99β side chain hydroxyl. Ring C of the tricycle stacks against the phenyl ring of Tyr166α. The 8-chloro substituent packs in a narrow groove (denoted α1, a mnemonic for halogen-binding pocket 1 of the α subunit, Figure 5B), and interacts directly with the face of the

Table 1. Summary of Data Collection and Crystallographic Refinement Statistics

	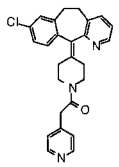	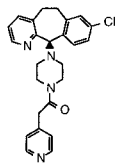	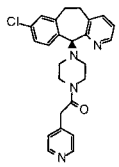	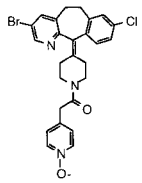	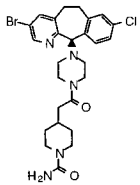	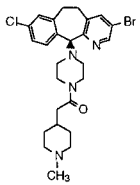	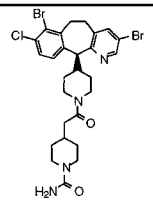	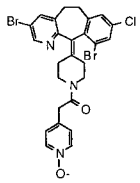	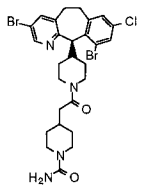	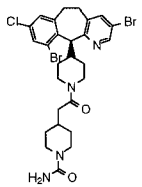
Inhibitor	**1**	**3**	**4**	**7**	**5**	**6**	**9**	**8**	**2**	**10**
IC_{50} (nM)	250	500	140	52	43	50	5.0	3.9	1.9	378
unit cell parameters										
a = b (Å)	171.2	171.4	171.2	171.3	171.2	171.0	172.5	170.9	171.1	171.4
c (Å)	69.2	69.2	69.3	69.2	69.2	69.2	69.5	69.2	69.3	69.2
number of reflections	66045	64786	64836	60501	62117	51086	54369	75123	49482	56631
(multiplicity)	(2.9)	(3.0)	(2.9)	(2.4)	(2.9)	(2.9)	(2.9)	(2.5)	(3.5)	(2.8)
resolution range (Å)	50 - 2.1	50 - 2.1	50 - 2.1	50 - 2.1	50 - 2.1	50 - 2.3	50.0 - 2.2	50 - 2.0	50 - 2.3	50 - 2.2
completeness (%)	97.8	95.9	96.3	89.8	92.6	99.1	90.5	96.4	95.9	95.8
(outer shell)	(89.4)	(81.9)	(84.1)	(70.6)	(71.4)	(92.7)	(75.5)	(85.7)	(71.9)	(75.6)
R_{merge} (%) (outer shell)	9.3 (28.1)	6.5 (21.8)	7.0 (23.3)	8.4 (14.7)	7.0 (20.2)	7.9 (38.3)	5.5 (38.2)	9.2 (33.1)	5.5 (21.1)	4.7 (22.3)
$\langle I \rangle / \langle \sigma_I \rangle$ (outer shell)	11.4 (2.5)	13.6 (3.6)	13.9 (3.3)	14.3 (5.0)	13.8 (3.5)	12.7 (1.9)	19.6 (1.9)	11.3 (2.8)	23.2 (4.8)	21.7 (3.1)
X-ray source	APS	APS	APS	APS	APS	Rigaku	Rigaku	APS	Rigaku	Rigaku
R_{factor} (%)	18.2	18.5	18.2	17.3	18.4	17.7	22.3	19.6	17.4	18.3
electron density (σ)										
8-Cl	11	11	14	22	11	10	16	13	11	11
3-Br	--	--	--	21	29	24	34	36	30	25
10-Br	--	--	--	--	--	--	32 (7-Br)	33	33	21
interring angle[a] (°)	--	67	66	--	73	73	78	--	77	88
<B-value> ($Å^2$)										
FPT	29	30	28	27	30	30	40	28	32	35
FPP	15	20	17	15	16	18	21	17	17	23
inhibitor	22	29	20	22	27	31	29	22	25	39
zinc	20	20	19	17	21	22	29	20	24	26
water	46	48	45	45	46	47	43	46	49	50

[a] Torsion angle between rings B and D.

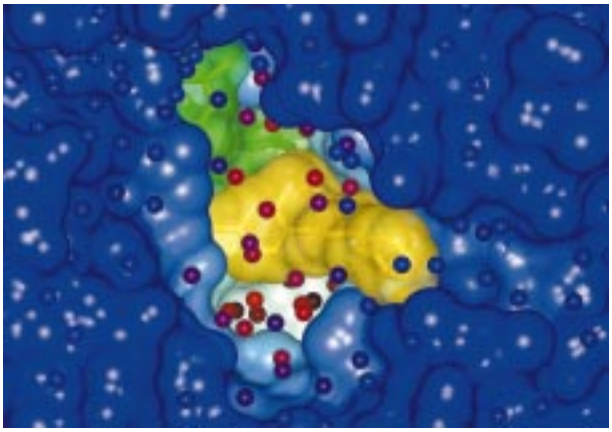

Figure 3. Space-filling view of the active site of FPT. Oxygen atoms of more than 70 discrete water molecules defined in the electron density are shown as isolated spheres. They are colored from dark-red to blue based upon their distance from the base of the active site. SCH 44342 (**1**) is shown in yellow. The FPP bound between SCH 44342 and FPT is in green. The displayed surfaces are defined by the solvent contact surface.[39]

Tyr166α aromatic ring and the edge of the His201α imidazole. Similar interactions between halogen atoms and side chain aromatic rings have been observed in other protein:inhibitor complexes, such as the herpes simplex virus type-I thymidine kinase complexed with 5-(bromothienyl)uracil [23] and haloalkane dehalogenase complexed with 1,2-dichloroethane.[24]

The planes of the piperidine ring (ring D) and tricycle are nearly perpendicular. The piperidine adopts a slightly twisted chair conformation and is within van der Waals contact of the Leu96*β* isopropyl, Tyr361*β* phenol, and Trp106*β* indole side chains. Only one side of the piperidine ring is exposed to solvent (Figure 3).

In the bound state, rings D and E of SCH 44342 are collinear and the plane of the pyridinyl ring (ring E) is rotated nearly 90° relative to the piperidine ring. The pyridinyl ring binds in a shallow groove (Figure 3) and forms a stacking interaction with Tyr93*β* (Figure 4). The ring also participates in two hydrogen bonds with discrete water molecules (Figure 4). One is hydrogen bonded to the pyridine nitrogen, and the other interacts with the face of the aromatic ring. Within this class of FPT inhibitors, only minor changes in potency resulted from substitutions on the pyridinyl ring (ring E). This SAR is consistent with the structure which shows that the pyridinyl ring is oriented toward solvent. For this reason, any pendant groups are also likely to be solvent exposed where, according to the existing SAR,[10,13] few energetically favorable interactions between inhibitor and FPT are made.

The amide carbonyl between rings D and E is required for high-affinity interactions with FPT.[10] In SCH 44342, the carbonyl oxygen acts as a hydrogen bond acceptor with a water molecule which is immobilized by hydrogen bonds to the backbone amide nitrogens of Phe360*β* and Tyr361*β* (Figure 4). Decreases in inhibitor affinity resulting from removal of the amide carbonyl likely reflect disruption of this well-defined hydrogen-bonding network. A single methylene between the amide carbonyl and the pyridinyl ring is optimal. Reductions in inhibitor potency that accompany alterations in the number of atoms between the amide carbonyl and pyridinyl ring could also reflect disruption of the stacking interactions of ring E with side chains of Tyr93*β* and Leu96*β*.

Inhibitor Interactions with FPP. The crystal structure also revealed several interactions between **1** and the bound FPP. In the complex, the pyridinyl ring of the tricycle (ring A, Figure 1) packs adjacent the third isoprenoid unit of FPP (Figure 4). Ring C interacts with the first isoprenoid unit, and the C-5 and C-6 carbons of the tricycle form van der Waals contacts with the second isoprenoid unit of FPP. The contact area between inhibitor rings A, B, and C and the hydrophobic farnesyl

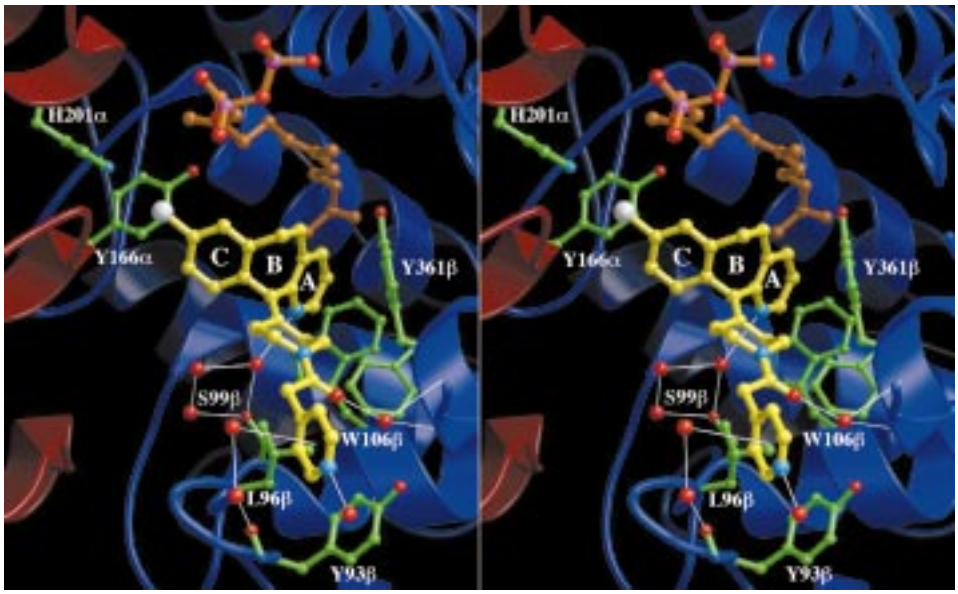

Figure 4. Stereoviews of the SCH 44342 (**1**):FPP:FPT ternary complex. In this and the remaining figures of the crystallographic structures, the inhibitor:FPP:FPT complex is represented in a standard format. Carbon atoms of the inhibitor and FPP are shown in yellow and orange, respectively. Spheres representing heteroatoms are colored red (oxygen), blue (nitrogen), white (chlorine), purple (phosphate), and bromine (orange). Thin white lines show hydrogen bonding between selected ordered water molecules and the inhibitor. Protein residues near the bound inhibitor are shown in green, and red and blue ribbons indicate FPT α and *β* subunits, respectively. Images were generated using MOLSCRIPT[40] and RASTER3D.[41]

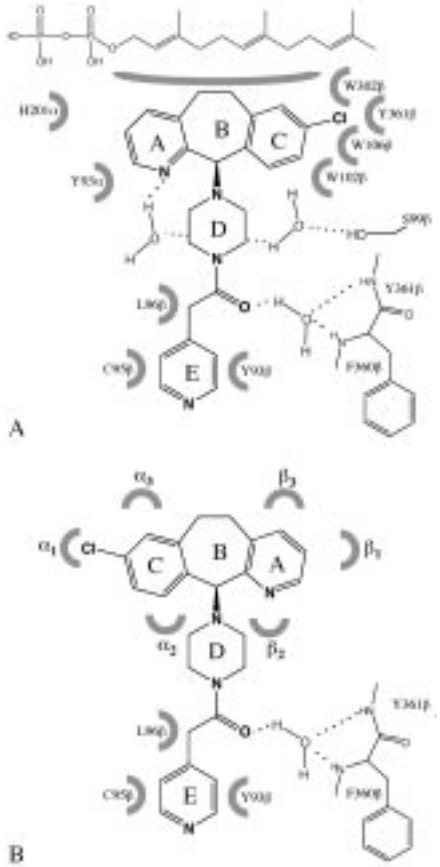

Figure 5. (A) Detailed interactions for **3**. (B) Binding orientation of **4** with the six halogen sites described throughout identified.

chain totals nearly 80 Å^2. Direct inhibitor and FPP interactions were unanticipated by kinetic measurements which show that the tricyclic compounds are competitive inhibitors of ras and ras-derived peptides.[14]

Together, SCH 44342 and FPP fill about one-third of the active site cavity and occupy approximately 360 and 320 Å^3, respectively. About 70 solvent molecules are localized in the remainder of the active site cavity (Figure 3). Calculations show that 30% and 10% of the SCH 44342 and FPP surfaces, respectively, remain exposed to solvent.

The tricyclic inhibitors bind the FPT:FPP complex with a ~10-fold increase in affinity relative to unliganded FPT. For example, in the absence of FPP, the K_d of binding for **7** is 540 nM as measured by ITC, whereas in the presence of a 1.6:1 molar excess of FPP over FPT, the affinity increases to 17.5 nM (Table 2). Dissociation constants computed from the free energies of binding for the latter association reaction are closer to the IC_{50}'s observed in enzymatic assays conducted with an excess of FPP. This suggests the inhibitor binds to the FPT:FPP complex. It has also been proposed that in vivo FPT predominately exists with FPP bound.[25] The prerequisite for FPP binding to achieve higher inhibitor affinity is similar to the situation of peptide binding to FPT. Enzymatic catalysis only occurs when the CaaX peptide binds to the FPT:FPP complex.[26,27]

Features of the ternary complex structure also suggest that the inhibitors bind a preformed FPT:FPP complex. First, the FPP binding site is located deeper in the active site cavity and situated between the tricycle and FPT. Second, the FPP conformation in the structures reported here is similar to that observed in the crystallographic structures of the FPT:FPP[28] and the FPT:α-hydroxyfarnesylphosphonic acid (αHFP): Cys-Val-Ile-Met complexes.[29] Taken together, these structures indicate that the bound conformation of FPP is relatively stable and essentially unperturbed upon binding of either peptide substrates or the tricyclic inhibitors.

Conformational Changes on Inhibitor Binding. Comparison of three crystal forms of FPT shows that few conformational changes occur when the tricycle inhibitors bind. The protein in the ternary inhibitor complexes reported here and the FPT:αHFP:CaaX peptide complex[29] superimpose with a 0.4 Å rms deviation. Small differences in overall protein structure are also observed when similar comparisons between the unliganded form[16] and the ternary complexes are made, although major rearrangements of some active site side chains occur on FPP binding.[29]

Interactions of Inhibitors Having Alternate Chiralities at C-11. To explore the SAR of SCH 44342 (**1**), piperizine analogues which differ in chirality at C-11 were synthesized. Surprisingly, both isomers retained high potency, although the *S* isomer was somewhat more active. For example, **3** and **4**, which differ only in chirality at C-11, inhibit FPT with IC_{50} values of 500 and 140 nM, respectively.

The crystal structures of the C-11 stereoisomers, **3** and **4**, each bound to FPT were compared to that of **1**. The binding modes of **1** and **4** are most similar. When the structures are superimposed, the 31 atoms of the inhibitors have an average rms deviation of 0.2 Å, which clearly shows that substitution of the double bond by the single bond minimally alters the overall conformation of the bound inhibitor.

The crystal structure of **3,** with the *R* isomer at C-11, shows this compound occupies the same binding site as the *S* isomer **4**. However, when complexed with FPT, the entire tricycle has rotated 180° relative to the active site (Figure 5A). The new orientation was clearly apparent in the initial electron density maps, which showed a 11σ difference peak corresponding to the 8-chloro substituent at the new position. The second halogen-binding site is located on the β-subunit and designated β1 (Figure 5B). Comparison of the bound conformations of **3** and **4** (Figure 5) shows that while the average change in atomic position is 5 Å, much larger movements are observed for some tricycle substituents. For example, the relative rotation of the tricycle moves the 8-chloro substituent 11 Å where it occupies the β1 pocket formed by the FPP isoprenoid and several aromatic side chains. Despite the rotation, the individual binding sites for inhibitor atoms remain occupied. For example, the position of C-9 in **3** is occupied by the C-2 atom of **4** (Figure 5).

In addition to a 180° relative rotation, the tricycle of **3** is translated about 0.35 Å relative to that of **4** (Figure 7A). Without translation, the chlorine atom would sterically overlap FPP. The change in tricycle orientation results in a 60° rotation of the peptide bond between Lys164α and Asn165α, and some movement in the first isoprenoid unit of FPP. Except for the small translation of the entire molecule and 180° relative rotation of the

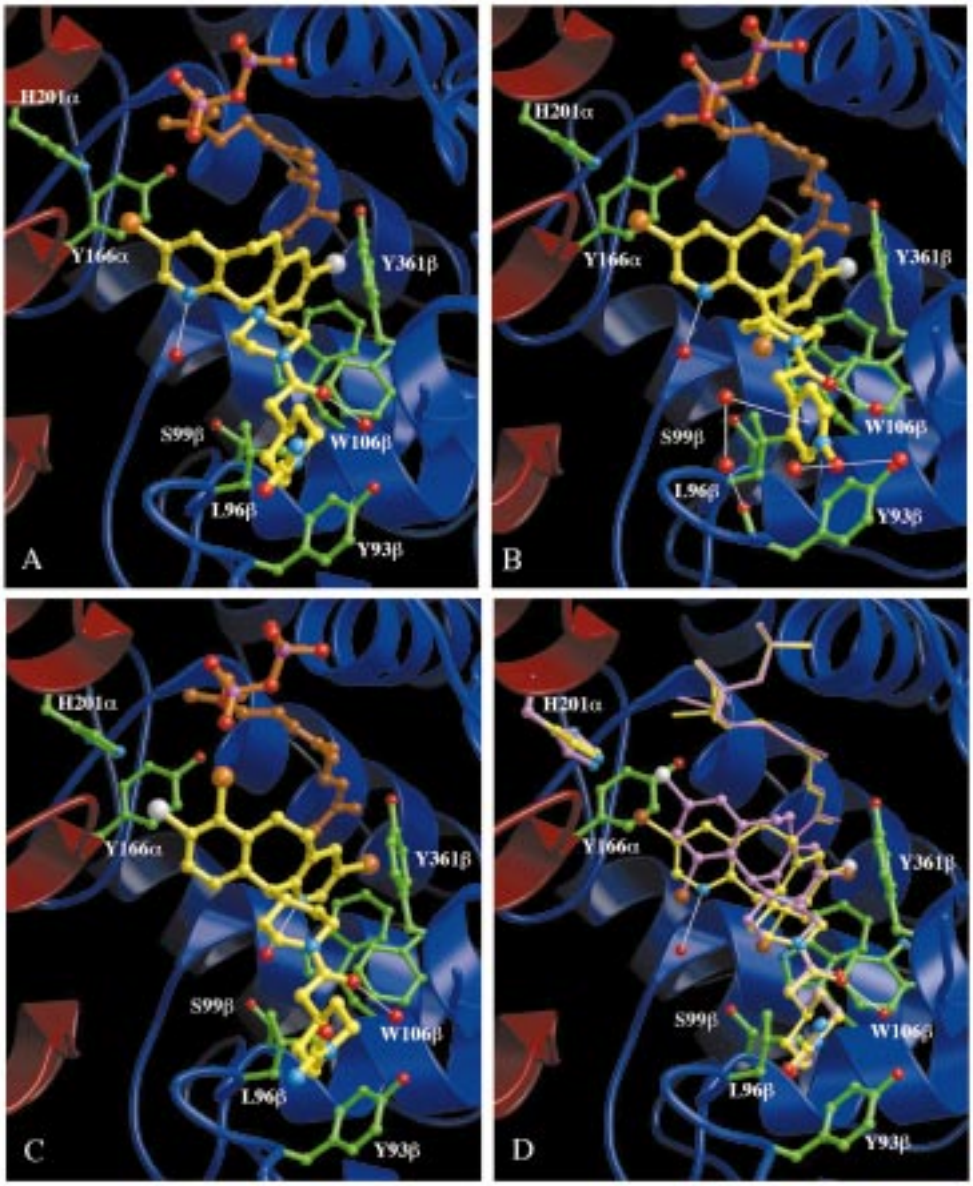

Figure 6. Structures of compound **5** (A), compound **8** (B), compound **9** (C), and compounds **2** (yellow) and **10** (purple) (D) bound to FPT.

tricycle, the overall binding mode of the inhibitor is largely unchanged (Figure 7A).

Binding of Dihalogen Tricycle Inhibitors. Potency of the monohalogen inhibitors was relatively insensitive to modification of rings D and E. However, addition of halogen substituents at the 3 position (ring A) increased affinity for FPT nearly 10-fold. Structural studies on the monohalogen inhibitors showed a well-conserved tricycle binding site on FPT and revealed two distinct halogen-binding pockets (α1 and β1), suggesting that both sites could be occupied simultaneously. Unlike the monohalogen series, dihalogen inhibitors with either configuration at C-11 were equipotent. Given the movements in FPP and FPT side chains to accommodate alternate orientations of the tricycle in the monohalogen series, crystallographic structures of a series of 3-Br, 8-Cl tricycle inhibitors (**5**−**7**) were undertaken to understand the differences in SAR for the mono- and dihalogenated inhibitors.

The structure of **5**, a 3-bromo 8-chloro tricyclic derivative with the *R* configuration at C-11, showed an inhibitor binding mode similar to that observed for the monohalogen series (Figure 6A). The electron density clearly showed locations for the two halogens with 29σ and 11σ peaks corresponding to the 3-bromo and 8-chloro atoms, respectively. These atoms occupied both the α1 and β1 pockets. When compared to **3**, the average rms change in equivalent atoms is less than 0.2 Å. Comparison of the structures also shows that for **5**, the 3-Br is essentially added to **3**. Ring E of **5** adopts a chair conformation with C-3 and C-5 away from the amide carbonyl (between rings D and E) to prevent intramolecular steric overlap. As a result, the urea group is oriented into bulk solvent. Unlike the solvent structure associated with the pyridine (ring E) of **1**, no water molecules are localized near the piperidine (ring E) of **5**.

In another cocrystal structure, the 3-bromo 8-chloro dihalogen inhibitor having the *S* chirality at C-11 (**6**) was shown to bind the FPT active site in an analogous fashion. Similar to bound monohalogen inhibitors, the orientations of the tricycle ring systems differ by 180°

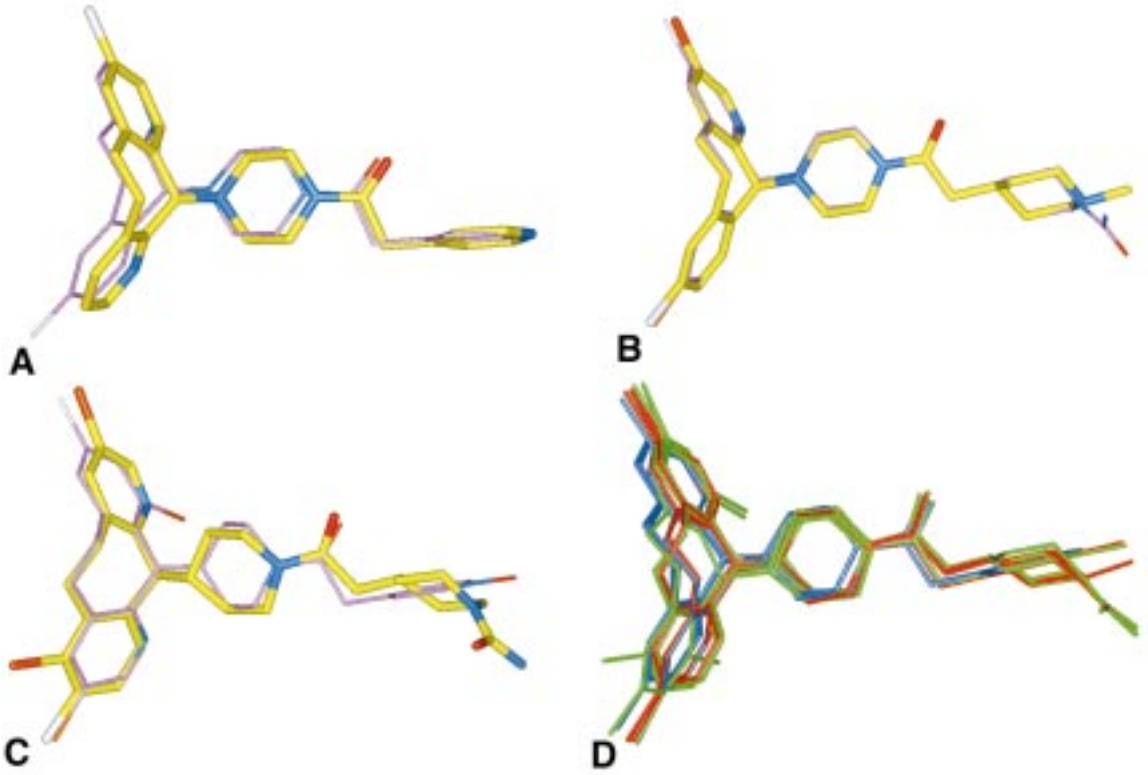

Figure 7. Overlay views of the bound conformations of compounds **3** (yellow) and **4** (purple) (A), compounds **5** (purple) and **6** (yellow) (B), compounds **9** (yellow) and **8** (purple) (C), and all the compounds in Table 1 where mono-, di-, and trihalogen inhibitors are colored blue, red, and green, respectively (D).

when the structures of compounds having opposite chiralities at C-11 are compared (Figure 7B). While the equivalent atoms have moved an average of 5 Å as observed in the comparison of the bound monohalogen inhibitors, no relative translation of the compounds is observed. Lack of relative changes in inhibitor orientation may reflect packing constraints imposed by the larger size of the inhibitor. The piperidine (ring E) adopts a chair conformation with the *N*-methyl group in the equatorial position. The *N*-methyl group interacts with Tyr93β, and the piperidine nitrogen is oriented toward bulk solvent.

Dihalogen compounds with opposite chiralities at C-11 exhibit distinct binding orientations. However, dihalogen inhibitors with a double bond between tricycle and piperidine ring (**7**) bind in both orientations. Evidence for dual binding modes comes from comparison of the electron density values for positive difference peaks. The electron density maps for **5** and **6** show approximately 3-fold higher difference peaks (30σ vs 10σ, Table 1) for the bromo and chloro atoms, respectively. The equivalent electron density values for halogen positions of **7** (Table 1) indicate that the tricycle of **7** binds with equal occupancy, both orientations observed for the single-bond compounds. The crystallographic data for **7** complexed with FPT also suggest that the sites occupied by the halogen atoms in compounds **5** and **6** bind the 3-bromo and 8-chloro substituents with comparable affinity. This finding is consistent with the thermodynamic binding parameters for **12** and **13**, members of the dihalogen series which differ only in stereochemistry at C-11. The enthalpies of binding for these compounds are within experimental error, while when complexed with FPT, the sites occupied by the 8-chloro and 3-bromo substituents in one stereoisomer are respectively occupied by the 3-bromo and 8-chloro substituents in the other.

Binding of Trihalogen Tricycle Inhibitors. Continued attempts to increase the potency of the mono- or dihalogen tricycles resulted in inhibitors with IC_{50} values near 50 nM.[9,13] To further increase affinity, sites for addition of substituents to the tricycle ring were explored. These studies resulted in the discovery that addition of halogens to either the 10 or 7 position of the tricycle increased potency 10-fold. The structures of several trihalogen tricycle inhibitors complexed with FPT were determined to understand their binding properties.

Figure 6B shows the bound conformation of **8** which is halogenated at the 3, 8, and 10 positions of the tricycle. On binding, the 10-bromo atom occupies the β2 pocket (Figure 5B) and makes van der Waals contacts with Trp102β and Trp106β. The 10-bromo substituent also displaces a water molecule which, in the mono- and dihalogen inhibitor structures, forms a 2.8 Å hydrogen bond to Ser99β (Figure 4). The conformation of Ser99β appears unchanged, and alternate hydrogen bonding to solvent is not observed. Instead, the serine hydroxyl is within 3.8 Å of the 10-bromo atom. The bound conformations of the piperidine and pyridine rings (D and E) of the inhibitor are similar to those observed in the previously described series.

Figure 6C shows the bound conformation of **9** which is halogenated at the 3, 7, and 8 positions of the tricycle. The 7-bromo atom of **9** binds in the α3 pocket (Figure 5B) and packs adjacent to the first isoprenoid unit of

Table 2. Thermodynamic Binding Parameters for Tricyclic Inhibitors

Inhibitor	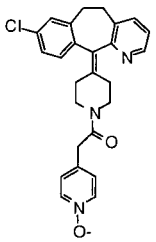	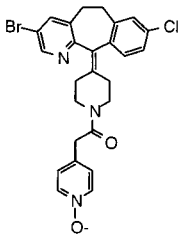	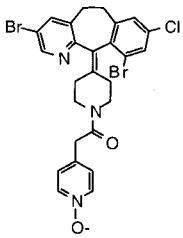	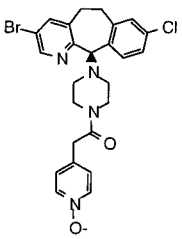	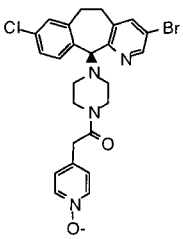
	11	**7**	**8**	**12**	**13**
IC_{50} (nM)	530	52	3.9	25	11
Kd (nM)	240 ± 23	17.5 ± 3	5.1 ± 0.8[a]	32.0 ± 4.6	21.0 ± 4.5
$\Delta G°_{bind}$ (kcal/mol)	-8.8 ± 0.8	-10.4 ± 1.8	-11.0 ± 1.8[a]	-10.0 ± 1.4	-10.2 ± 2.1
$\Delta H°_{bind}$ (kcal/mol)	-9.8 ± 0.1	-10.5 ± 0.1	-12.5 ± 0.1	-11.6 ± 0.1	-11.2 ± 0.1
$T\Delta S°_{bind}$ (kcal/mol)	-1.0 ± 0.8	-0.1 ± 1.8	-1.5 ± 1.8[a]	-1.6 ± 1.4	-1.0 ± 2.1

[a] Fitted values are near the limit of accuracy for high-affinity compounds.[31]

FPP, which along with the imidazole ring of His201α has shifted slightly to accommodate the bromine. Comparison of **9** and **8** (Figure 7C) suggests that a tetrahalogenated compound would further improve potency. Compound **9** with the *S* chirality at C-11 exhibits an IC_{50} of 5.0 nM, while the compound with the *R* isomer at C-11 has an IC_{50} of 78.0 nM.[8] If the latter compound binds with the tricycle rotated 180° relative to the bound *S* isomer as seen for the dihalogenated tricyclic inhibitors, the lower affinity could reflect steric overlap between the 8-bromo and protein atoms in the β3 pocket.

A major step toward finding a FPT inhibitor useful as a drug was the discovery of SCH 66336 (**2**), a 3,10-dibromo 8-chloro tricycle. SCH 66336 was found to have excellent preclinical characteristics and is now in clinical trials as an anticancer agent. Crystallographic analyses reveal that SCH 66336 binds in the FPT active site cavity. The compound spans the active site and interacts directly with atoms of the enzyme and bound solvent molecules. Unexpectedly, the inhibitor SCH 66336 also packs against the isoprenoid chain of FPP. The overall binding mode is similar to that observed for other tricyclic inhibitors (Figure 6D). The three halogen atoms pack against aromatic side chains in well-defined pockets, with the 10-bromo in the β2 pocket as observed for **8**. The piperidine ring (ring D) is nearly perpendicular to the tricycle, similar to the piperazine rings in the mono- and dihalogen inhibitors; however, it is rotated 77° relative to the plane of the tricycle (Table 1), slightly more than in the mono- and dihalogen inhibitors.

The chirality of C-11 in SCH 66336 (**2**) is *R*, and the compound inhibits FPT with an IC_{50} of 1.9 nM. The corresponding inhibitor with the C-11 *S* isomer (**10**) binds ~200-fold weaker (IC_{50} = 378 nM, Table 1). Crystal structures of each compound complexed with FPT show that while both occupy the same region of the active site, the tricycle ring orientations in the bound compounds differ by 180° (Figure 6D). In the case of the dihalogen inhibitors which are approximately 2-fold symmetric about C-11, both C-11 isomers were equipotent and exhibited very similar binding patterns when complexed with FPT. For the trihalogen inhibitors, neither trend is observed. Comparison of the structures of **2** and **10** complexed with FPT revealed that the tricycle ring orientation differs by 180° for the compounds with *R* and *S* isomers at C-11 (**2** and **10**, respectively). In addition, the tricycle system of **10** complexed with FPT is rotated ~11° relative to that in the FPT complex with **2** (Figure 6D), and the tricycle pivots about the C-8 atom of **2**. As a result, the 8-chloro and 3-bromo substituents of **2** and **10**, respectively, occupy the same binding pocket in FPT, while the 8-chloro and 3-bromo substituents of **10** and **2**, respectively, occupy sites that are 2.2 Å apart. This 12° rotation is compensated for by the torsion angle between the tricycle and ring D (Table 1), so that the binding sites of the E rings of **2** and **10** are virtually identical. The 10-bromo in **10** now occupies a new halogen-binding pocket (α2).

Conserved Hydrogen Bonds. Hydrogen-bonding patterns to the pyridine nitrogen atom of the tricycle and the amide carbonyl between rings D and E are conserved in the inhibitor:FPT complexes. In both cases, inhibitor atoms are bonded to discrete water molecules which are apparently located in the active site prior to inhibitor binding, since water molecules in similar locations are observed in the refined structures of unliganded FPT[16] and FPT complexed with a peptide substrate.[29]

The inhibitor amide carbonyl participates in a water-mediated hydrogen bond network involving two protein

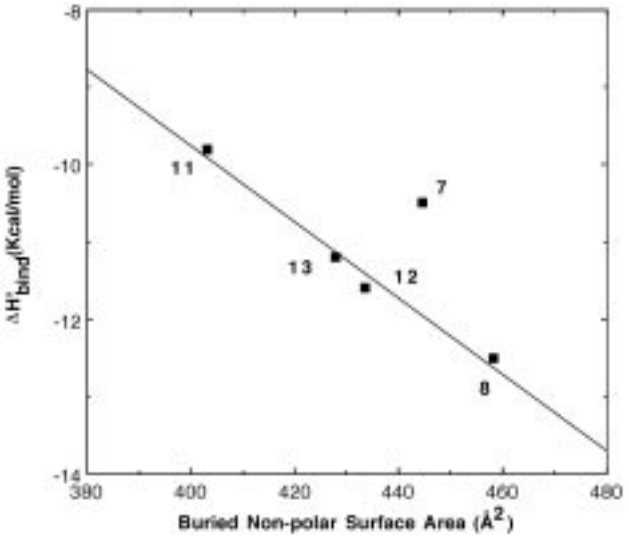

Figure 8. Plot of buried nonpolar surface area versus the $\Delta H°_{bind}$. The individual compounds from Table 2 are labeled. Surface areas were calculated with Insight 97.2 with halogen atoms considered as nonpolar (MSI Inc.). Compound **7** is an outlier. This is possibly due to the fact that it possesses multiple binding modes and/or that the double-bond dihalogen tricycles do not pack as efficiently in the active site.

backbone amides. The intervening water molecule serves as a hydrogen bond donor to the inhibitor carbonyl and acts as a hydrogen bond acceptor for two backbone amide nitrogens. Thus, the well-localized water molecule is optimally oriented to serve as a hydrogen bond donor to the inhibitor amide carbonyl.

Nearly 70 discrete water molecules are ordered near the bound tricycle and within the FPT active site cavity (Figure 3). Only minor changes in water positions accompany hydrogen bond formation between the pyridine nitrogen of tricycle ring A and an ordered water. In the FPT complexes with **1**, **4**, **6**, **9**, and **10**, a water molecule hydrogen bonded to the tricycle nitrogen heteroatom is centrally located within a large cluster of water molecules, while in the complexes with **2**, **3**, **5**, **7**, and **8**, a water molecule interacting with the nitrogen of ring A is also hydrogen bonded to the Ser99β side chain hydroxyl (Figure 5A). However, in the complexes with **2** and **8,** the water molecule directly bonded to the Ser99β hydroxyl is displaced by the 10-Br substituent without major adjustments in the positions of the other water molecules in the active site (Figure 6D).

Thermodynamic Binding Parameters. Association of the tricycle inhibitors with the FPT:FPP complex is enthalpically favored. For example, $\Delta H°_{bind} = -9.8 \pm 0.1$ kcal/mol and $T\Delta S°_{bind} = -1.0 \pm 0.8$ kcal/mol for **11** (Table 2). Inspection of the structure indicates that the favorable enthalpic contributions arise from extensive van der Waals contacts between the inhibitor and both FPT and FPP. Association of compound **11** buries approximately 460 Å^2 of surface area, roughly 90% of which is nonpolar. The buried nonpolar surface area increases with the addition of each halogen, and the incremental increases correlate with increases in $\Delta H°_{bind}$ (Figure 8). For each additional 20 Å^2 of buried nonpolar surface area, an additional 1 kcal/mol in $\Delta H°_{bind}$ is observed. This is consistent with the range measured for aliphatic groups.[30−32] Electrostatic interactions, including hydrogen bonding to the inhibitor carbonyl and edge-to-face interactions of rings A and C with protein aromatic residues, also contribute to the overall favorable $\Delta H°_{bind}$.

Complex formation between tricycle inhibitors and the FPT:FPP complex occurs with minimal changes in overall entropy. As shown in Table 2, $T\Delta S°_{bind}$ ranges from -0.1 ± 1.8 to -1.6 ± 1.4 kcal/mol. The minimal overall change indicates that entropically favorable effects such as solvent displacement from inhibitor and FPT are nearly offset by disfavored effects including losses of internal conformational degrees of freedom in both inhibitor and enzyme.

Discussion

The structures of representative FPT inhibitors of the tricycle family revealed the inhibitor binding orientation within the active site cavity of FPT (Figure 7D). The tricyclic moiety spans a hydrophobic region at the base of the active site. Rings D and E adopt an extended conformation and bind roughly perpendicular to the tricycle. Ring E is oriented toward bulk solvent. Water-mediated hydrogen bonding to the pyridine nitrogen of the tricycle and the amide carbonyl between rings D and E is preserved in the FPT:FPP:inhibitor complexes. Most inhibitors bind without significant alteration of the overall FPT structure. The crystal structures showed that the C-5 and C-6 tricycle atoms and, in some cases, the halogen substituents form van der Waals packing interactions with the bound FPP. The hydrophobic interactions likely account for the consistent observation that inhibitors bind the FPT:FPP complex more tightly than unliganded FPT.

The thermodynamic binding parameters for complex formation between tricycle inhibitors and FPT provide a basis for understanding the observed structures. The free energy of complex formation is enthalpically favorable, which, the structures suggest, reflects van der Waals packing and hydrogen-bonding interactions. The correlation between more favorable enthalpies of binding and increases in inhibitor potency accompanying addition of halogen substituents to the tricycle is especially striking. To a first approximation, the close correspondence is due to increased hydrophobic packing interactions between inhibitor and the FPT:FPP complex. The favorable enthalpy contributions to complex formation are also likely to reflect preservation of hydrogen-bonding to polar atoms of the bound inhibitor. For example, similar hydrogen bonding interactions are possible between the amide carbonyl in solution and in the FPT:FPP:inhibitor complex.

In conclusion, tricyclic inhibitors are potent, selective FPT inhibitors, one of which, SCH 66336 (**2**), is in clinical trials.[15] These inhibitors demonstrate a remarkable fit in the FPT active site and maintain a conserved binding mode even with major alterations in stereochemistry. The crystallographic structures have revealed the detailed interactions between the tricycle inhibitors and FPT and provided a structural rationale for the observed SAR. Together with the thermodynamic analyses, these studies have provided a clear framework for elaboration of the tricycle series of inhibitors.

Experimental Section

Protein Crystallization. Crystals of FPT:FPP:inhibitor complexes were prepared by either cocrystallization or soaking

compounds into preformed crystals. For soaking experiments (**1**, **3**−**5**, **7**, **8**, **10**), crystals of the αHFP:peptide:FPT complex[33] were soaked in inhibitor-containing solutions. Crystals measuring about 100 × 100 × 300 μm were transferred into 300 μL of the reservoir solution supplemented with 10 μM $ZnCl_2$, 2 mM DTT, 100 μM FPP, and 100 μM inhibitor. The mixture was allowed to equilibrate for 24 h at 4 °C. Using this procedure, the FPP analogue and peptide are displaced by FPP and inhibitor. Cocrystals of compounds **6** and **2** were obtained as previously described[33] by substituting FPP for αHFP and **6** or **2** for the CVIM peptide. Cocrystals of **9** were obtained under different conditions[29] with FPP replacing αHFP and **9** replacing the CVIM peptide.

Prior to data collection, crystals were taken from the crystallization droplet or soaking solution and flash-frozen in liquid propane using a cryoprotectant consisting of the reservoir solution supplemented with 40% (v/v) glycerol. Crystals belong to space group $P6_1$ and contain one FPT molecule per crystallographic asymmetric unit. Diffraction limits and unit cell parameters for crystals used in these studies are given in Table 1.

Data Collection. X-ray diffraction data were collected using both rotating anode and synchrotron sources. For the former, an Raxis-IIc image plate area detector was mounted on a Rigaku-R200 rotating anode X-ray generator operating at 50 kV and 100 mA. The X-ray beam intensity was increased by focusing with "bent mirrors" (J. Johnson and Dr. Z. Otwinowski, Yale University; Molecular Structure Corp.). With the detector set at $2\theta = 0°$ and a crystal-to-detector distance of 135 mm, data were collected in 180 contiguous 0.30° oscillation images each exposed for 12 min. A Brüker 2 × 2 CCD detector was used for data collection at the Advanced Photon Source Sector-17 (Chicago, IL); 175 contiguous 0.3° oscillation images each exposed for 5 s were collected with the detector set at $2\theta = -4°$ and 16.0 cm from the sample. Diffraction intensities were reduced to structure factors using HKL,[34] and data statistics are given in Table 1.

Structure Determination and Refinement. Coordinates of FPT were taken from an unrefined 2.9 Å resolution structure of unliganded FPT[16] and independently refined to 2.5 Å. This structure was used as the starting model for refinement of the first inhibitor:FPP:FPT complex. Following removal of the inhibitor and solvent molecules located near the active site, the remaining FPT:FPP model was used as the starting point for subsequent inhibitor:FPP:FPT complex structure determinations. After rigid body refinement, inhibitors were built into the initial omit density[35] in which the orientation of the complete inhibitor structure was usually very well-defined. Placement of inhibitors was aided by large difference peaks corresponding to the halogen substituents, which were over 30σ in some cases. Refinement of the final model included several cycles of model building and positional refinement using XPLOR.[36] Positions of discrete water molecules were taken from positive $3\sigma\,(F_o - F_c)\alpha_{calc}$ difference density peaks if a hydrogen-bonding pattern to protein, peptide, or solvent atoms could be established. Refinement was carried out using data from 8 Å to the resolution limit of the data and a 1 I/σ_I cutoff. Refinement statistics are shown in Table 1. Electron density and structure analyses were carried out using programs CHAIN,[37] QUANTA (Molecular Simulations Inc.), and INSIGHT (Molecular Simulations Inc.).

Isothermal Titration Calorimetry. Heats of complex formation were measured by titrating the concentrated inhibitor into a protein solution using an isothermal titration calorimeter (MCS, MicroCal Corp., Northampton, MA). Binding curves usually involved the addition of 20−25 12-μL injections which enabled 50% saturation to occur by the tenth injection. Baseline correction for heats of dilution, typically −0.1 μcal/s, involved subtracting values obtained by titrating the inhibitor solution into the reaction cell containing all but the protein or by subtracting values obtained following saturation in the binding curve. The syringe mixing speed was 250 rpm, and data were recorded at the 20% reference offset in order to maximize the signal-to-noise ratio. The time between injections was 300 s. Nonlinear least-squares analysis of the binding curve yielded values for thermodynamic parameters of binding and inhibitor-to-FPT stoichiometry (ITC Origin Program, V2.8, MicroCal Corp., Northampton, MA). The data fit well to a single binding site mechanism with stoichiometry values corresponding to a 1:1 interaction between inhibitor and FPT.

For ITC experiments, human FPT was expressed in bacculovirus, purified and assayed as previously described.[14] FPT samples were dialyzed against two changes of buffer (40 mM Hepes, 1 mM DTT, pH 7.4 (buffer A) at 20 °C) and frozen at −20 °C in aliquots sufficient for a single titration experiment. The dialysate was filtered and frozen in 15-mL aliquots. FPT samples were centrifuged, and both inhibitor and protein solutions were degassed prior to loading into the syringe and reaction cell. The concentration of FPT was selected to have a c value between 1 and 1000 to facilitate accurate K_d determinations.[38] FPT concentrations were determined using A_{280} values ($\epsilon = 1.64$ mg^{-1} cm^2 (153 000 M^{-1} cm^{-1})). Because inhibitors typically exhibit 10-fold greater affinity for the FPP:FPT complex than for FPT, the 10 μM FPT solution was saturated with 16 μM FPP prior to injection of inhibitor. Lyophilized inhibitors were initially dissolved in DMSO to make a 7−20 mM solution. The concentrated inhibitor solution was diluted into the dialysate to yield final inhibitor and DMSO concentrations between 80 and 120 μM and 0.5−1%, respectively. DMSO was added to the FPT solution to equalize DMSO concentrations in the syringe and reaction cell. Similarly, the inhibitor solution was made 16 μM in FPP. FPT samples were centrifuged, and both inhibitor and protein solutions were degassed prior to loading into the syringe and reaction cell. Inhibitors were titrated into the protein-containing reaction cell (∼1.4 mL) using a 250-μL syringe. Thermodynamic binding parameters for representative tricyclic FPT inhibitors are summarized in Table 2.

Acknowledgment. We thank R. Syto and M. Demma for purification of FPT and the IMCA-CAT staff for assistance in the collection and processing of the APS data.

References

(1) Barbacid, M. Ras genes. *Annu. Rev. Biochem.* **1987**, *56*, 779−827.
(2) Willumsen, B. M.; Christensen, A.; Hubert, N. L.; Papageorge, A. G.; Lowy, D. R. The P21 Ras C-terminus is required for transformation and membrane association. *Nature* **1984**, *310*, 583−586.
(3) Reiss, Y.; Goldstein, J. L.; Seabra, M. C.; Casey, P. J.; Brown, M. S. Inhibition of purified p21ras farnesyl:protein transferase by Cys-AAX tetrapeptides. *Cell* **1990**, *62*, 81−88.
(4) Leonard, D. M. Ras farnesyltransferase: a new therapeutic target. *J. Med. Chem.* **1997**, *40*, 2971−2990.
(5) Casey, P. J.; Seabra, M. C. Protein prenyltransferases. *J. Biol. Chem.* **1996**, *271*, 5289−5292.
(6) James, G. L.; Goldstein, J. L.; Brown, M. S.; Rawson, T. E.; Somers, T. C.; McDowell, R. S.; Crowley, C. W.; Lucas, B. K.; Levinson, A. D.; Marsters, J. C., Jr. Benzodiazepine peptidomimetics: potent inhibitors of Ras farnesylation in animal cells. *Science* **1993**, *260*, 1937−1942.
(7) Kohl, N. E.; Mosser, S. D.; deSolms, S. J.; Giuliani, E. A.; Pompliano, D. L.; Graham, S. L.; Smith, R. L.; Scolnick, E. M.; Oliff, A.; Gibbs, J. B. Selective inhibition of ras-dependent transformation by a farnesyltransferase inhibitor. *Science* **1993**, *260*, 1934−1937.
(8) Njoroge, F. G.; Taveras, A. G.; Kelly, J.; Remiszewski, S.; Mallams, A. K.; Wolin, R.; Afonso, A.; Cooper, A. B.; Rane, D. F.; Liu, Y.; Wong, J.; Vibulbhan, B.; Pinto, P.; Deskus, J.; Alvarez, C. S.; del Rosario, J.; Connolly, M.; Wang, J.; Desai, J.; Rossman, R. R.; Bishop, W. R.; Patton, R.; Wang, L.; Kirschmeier, P.; Bryant, M. S.; Nomeir, A. A.; Lin, C.; Liu, M.; McPhail, A. T.; Doll, R. J.; Girijavallabhan, V. M.; Ganguly, A. K.(+)-4-[2-[4-(8-Chloro-3,10-dibromo-6,11-dihydro-5H-benzo[5,6]-cyclohepta[1,2-b]pyridin-11(R)-yl)-1-piperidinyl]-2-oxoethyl]-1-piperidinecarboxamide (SCH-66336): A Very Potent Farnesyl Protein Transferase Inhibitor as a Novel Antitumor Agent. *J. Med. Chem.* **1998**, *41*, 4890−4902.
(9) Njoroge, F. G.; Vibulbhan, B.; Rane, D. F.; Bishop, W. R.; Petrin, J.; Patton, R.; Bryant, M. S.; Chen, K. J.; Nomeir, A. A.; Lin, C. C.; Liu, M.; King, I.; Chen, J.; Lee, S.; Yaremko, B.; Dell, J.; Lipari, P.; Malkowski, M.; Li, Z.; Catino, J.; Doll, R. J.; Girijav-

allabhan, V.; Ganguly, A. K. Structure−activity relationship of 3-substituted N−(pyridinylacetyl)-4- (8-chloro-5,6-dihydro-11H-benzo[5,6]cyclohepta[1,2-b]pyridin-11-ylidene)piperidine inhibitors of farnesyl-protein transferase: design and synthesis of in vivo active antitumor compounds. *J. Med. Chem.* **1997**, *40*, 4290−4301.

(10) Njoroge, F. G.; Doll, R. J.; Vibulbhan, B.; Alvarez, C. S.; Bishop, W. R.; Petrin, J.; Kirschmeier, P.; Carruthers, N. I.; Wong, J. K.; Albanese, M. M.; Piwinski, J. J.; Catino, J.; Girijavallabhan, V.; Ganguly, A. K. Discovery of novel nonpeptide tricyclic inhibitors of Ras farnesyl protein transferase. *Bioorg. Med. Chem.* **1997**, *5*, 101−113.

(11) Njoroge, F. G.; Vibulbhan, B.; Pinto, P.; Bishop, W. R.; Bryant, M. S.; Nomeir, A. A.; Lin, C.; Liu, M.; Doll, R. J.; Girijavallabhan, V.; Ganguly, A. K. Potent, selective, and orally bioavailable tricyclic pyridyl acetamide *N*-oxide inhibitors of farnesyl protein transferase with enhanced in vivo antitumor activity. *J. Med. Chem.* **1998**, *41*, 1561−1567.

(12) Mallams, A. K.; Njoroge, F. G.; Doll, R. J.; Snow, M. E.; Kaminski, J. J.; Rossman, R. R.; Vibulbhan, B.; Bishop, W. R.; Kirschmeier, P.; Liu, M.; Bryant, M. S.; Alvarez, C.; Carr, D.; James, L.; King, I.; Li, Z.; Lin, C. C.; Nardo, C.; Petrin, J.; Remiszewski, S. W.; Taveras, A. G.; Wang, S.; Wong, J.; Catino, J.; Girijavallabhan, V.; Ganguly, A. K. Antitumor 8-chlorobenzocycloheptapyridines: a new class of selective, nonpeptidic, nonsulfhydryl inhibitors of ras farnesylation. *Bioorg. Med. Chem.* **1997**, *5*, 93−99.

(13) Mallams, A. K.; Rossman, R. R.; Doll, R. J.; Girijavallabhan, V. M.; Ganguly, A. K.; Petrin, J.; Wang, L.; Patton, R.; Bishop, W. R.; Carr, D. M.; Kirschmeier, P.; Catino, J. J.; Bryant, M. S.; Chen, K. J.; Korfmacher, W. A.; Nardo, C.; Wang, S.; Nomeir, A. A.; Lin, C. C.; Li, Z.; Chen, J.; Lee, S.; Dell, J.; Lipari, P.; Malkowski, M.; Yaremko, B.; King, I.; Liu, M. Inhibitors of farnesyl protein transferase. 4-Amido, 4-carbamoyl, and 4-carboxamido derivatives of 1-(8-chloro-6,11-dihydro-5H-benzo-[5,6]- cyclohepta[1,2-b]pyridin-11-yl)piperazine and 1-(3-bromo-8-chloro-6,11- dihydro-5H-benzo[5,6]cyclohepta[1,2-b]pyridin-11-yl)piperazine. *J. Med. Chem.* **1998**, *41*, 877−893.

(14) Bishop, W. R.; Bond, R.; Petrin, J.; Wang, L.; Patton, R.; Doll, R.; Njoroge, G.; Catino, J.; Schwartz, J.; Windsor, W.; Syto, R.; Schwartz, J.; Carr, C.; James, L.; Kirschmeier, P. Novel tricyclic inhibitors of farnesyl protein transferase. Biochemical characterization and inhibition of Ras modification in transfected Cos cells. *J. Biol. Chem.* **1995**, *270*, 30611−30618.

(15) Liu, M.; Bryant, M. S.; Chen, J.; Lee, S.; Yaremko, B.; Lipari, P.; Malkowski, M.; Ferrari, E.; Nielsen, L.; Prioli, N.; Dell, J.; Sinha, D.; Syed, J.; Korfmacher, W. A.; Nomeir, A. A.; Lin, C. C.; Wang, L.; Taveras, A. G.; Doll, R. J.; Njoroge, F. G.; Mallams, A. K.; Remiszewski, S.; Catino, J. J.; Girijavallabhan, V. M.; Kirschmeier, P.; Bishop, W. R. Antitumor activity of SCH 66336, an orally bioavailable tricyclic inhibitor of farnesyl protein transferase, in human tumor xenograft models and wap-ras transgenic mice. *Cancer Res.* **1998**, *58*, 4947−4956.

(16) Park, H. W.; Boduluri, S. R.; Moomaw, J. F.; Casey, P. J.; Beese, L. S. Crystal structure of protein farnesyltransferase at 2.25 angstrom resolution. *Science* **1997**, *275*, 1800−1804.

(17) Bradshaw, J. M.; Grucza, R. A.; Ladbury, J. E.; Waksman, G. Probing the "two-pronged plug two-holed socket" model for the mechanism of binding of the Src SH2 domain to phosphotyrosyl peptides: a thermodynamic study. *Biochemistry* **1998**, *37*, 9083−9090.

(18) Connelly, P. R.; Thomson, J. A. Heat capacity changes and hydrophobic interactions in the binding of FK506 and rapamycin to the FK506 binding protein. *Proc. Natl. Acad. Sci. U.S.A.* **1992**, *89*, 4781−4785.

(19) Luque, I.; Gomez, J.; Semo, N.; Freire, E. Structure-based thermodynamic design of peptide ligands: Application to peptide inhibitors of the aspartic protease endothiapepsin. *Proteins* **1998**, *30*, 74−85.

(20) McNemar, C.; Snow, M. E.; Windsor, W. T.; Prongay, A.; Mui, P.; Zhang, R.; Durkin, J.; Le, H. V.; Weber, P. C. Thermodynamic and structural analysis of phosphotyrosine polypeptide binding to Grb2-SH2. *Biochemistry* **1997**, *36*, 10006−10014.

(21) Tsai, F. T.; Singh, O. M.; Skarzynski, T.; Wonacott, A. J.; Weston, S.; Tucker, A.; Pauptit, R. A.; Breeze, A. L.; Poyser, J. P.; O'Brien, R.; Ladbury, J. E.; Wigley, D. B. The high-resolution crystal structure of a 24-kDa gyrase B fragment from E. coli complexed with one of the most potent coumarin inhibitors, clorobiocin. *Proteins* **1997**, *28*, 41−52.

(22) Weber, P. C.; Pantoliano, M. W.; Simons, D. M.; Salemme, F. R. Structure-Based design of synthetics azobenzene ligands for streptavidin. *J. Am. Chem. Soc.* **1994**, *116*, 2717−2723.

(23) Champness, J. N.; Bennett, M. S.; Wien, F.; Visse, R.; Summers, W. C.; Herdewijn, P.; de Clerq, E.; Ostrowski, T.; Jarvest, R. L.; Sanderson, M. R. Exploring the active site of herpes simplex virus type-I thymidine kinase by X-ray crystallography of complexes with aciclovir and other ligands. *Proteins* **1998**, *32*, 350−361.

(24) Verschueren, K. H.; Seljee, F.; Rozeboom, H. J.; Kalk, K. H.; Dijkstra, B. W. Crystallographic analysis of the catalytic mechanism of haloalkane dehalogenase. *Nature* **1993**, *363*, 693−698.

(25) Tschantz, W. R.; Furfine, E. S.; Casey, P. J. Substrate binding is required for release of product from mammalian protein farnesyltransferase. *J. Biol. Chem.* **1997**, *272*, 9989−9993.

(26) Furfine, E. S.; Leban, J. J.; Landavazo, A.; Moomaw, J. F.; Casey, P. J. Protein farnesyltransferase: kinetics of farnesyl pyrophosphate binding and product release. *Biochemistry* **1995**, *34*, 6857−6862.

(27) Pompliano, D. L.; Schaber, M. D.; Mosser, S. D.; Omer, C. A.; Shafer, J. A.; Gibbs, J. B. Isoprenoid diphosphate utilization by recombinant human farnesyl:protein transferase: interactive binding between substrates and a preferred kinetic pathway. *Biochemistry* **1993**, *32*, 8341−8347.

(28) Long, S. B.; Casey, P. J.; Beese, L. S. Cocrystal structure of protein farnesyltransferase complexed with a farnesyl diphosphate substrate. *Biochemistry* **1998**, *37*, 9612−9618.

(29) Strickland, C. L.; Windsor, W. T.; Syto, R.; Wang, L.; Bond, R.; Wu, Z.; Schwartz, J.; Le, H. V.; Beese, L. S.; Weber, P. C. Crystal structure of farnesyl protein transferase complexed with a CaaX peptide and farnesyl diphosphate analogue. *Biochemistry* **1998**, *37*, 16601−16611.

(30) Makhatadze, G. I.; Privalov, P. L. Contribution of hydration to protein folding thermodynamics I. The enthalpy of hydration. *J. Mol. Biol.* **1993**, *232*, 639−659.

(31) Murphy, K. P.; Gill, S. J. Thermodynamics of dissolution of solid cyclic dipeptides containing hydrophobic side groups. *J. Chem. Thermodyn.* **1989**, *21*, 903−913.

(32) Chothia, C. Hydrophobic bonding and accessible surface area of proteins. *Nature* **1974**, *248*, 338−339.

(33) Wu, Z.; Demma, M.; Strickland, C. L.; Syto, R.; Le, H. V.; Weber, P. C.; Windsor, W. T. High-level expression, purification, kinetic characterization and crystallization of protein farnesyltransferase β-subunit C-terminal mutants. *Protein Eng.* **1999**, *12*, 341−348.

(34) Otwinowski, Z.; Minor, W. Processing of X-ray diffraction data collected in oscillation mode. In *Methods in Enzymology*; Carter, C. W., Sweet, R. M., Eds.; Academic Press: New York, 1997; Vol. 276, pp 307−326.

(35) Bhat, T. N.; Ammon, H. L.; Mazzocchi, P. H.; Oda, M. Structure of 5-hydroxy-5-phenyl-7-azatricyclo[7.4.0.02,7]trideca-2,9(1),10,-12-tetraen-8-one by the consistent electron density approach. *Acta Crystallogr. C* **1990**, *46*, 116−119.

(36) Brünger, A. T.; Kuriyan, J.; Karplus, M. Crystallographic R Factor Refinement by Molecular Dynamics. *Science* **1987**, *235*, 458−460.

(37) Sack, J. S. CHAIN − A Crystallographic Modeling Program. *J. Mol. Graph.* **1988**, *6*, 224−225.

(38) Wiseman, T.; Williston, S.; Brandts, J. F.; Lin, L. N. Rapid measurement of binding constants and heats of binding using a new titration calorimeter. *Anal. Biochem.* **1989**, *179*, 131−137.

(39) Connolly, M. L. Solvent-accessible surfaces of proteins and nucleic acids. *Science* **1983**, *221*, 709−713.

(40) Kraulis, P. J. MOLSCRIPT: a program to produce both detailed and schematic plots of potein structures. *J. Appl. Crystallogr.* **1991**, *24*, 946−950.

(41) Merritt, E. A.; Murphy, M. E. P. Raster3D Version 2.0. A program for photorealistic molecular graphics. *Acta Crystallogr. Sect. D Biol. Crystallogr.* **1994**, *50*, 869−873.

JM990030G